

Curious case of gravitational lensing by binary black holes: a tale of two photon spheres, new relativistic images and caustics.

¹Mandar Patil^a, ²Priti Mishra^b, ³D Narasimha^c

¹*Institute of Mathematics of Polish Academy of Sciences,
Sniadeckich 8, 00-956 Warsaw, Poland.*

²*Harish-Chandra Research Institute, Chhatnag Road, Jhansi, Allahabad-211019, India.*

³*Tata Institute of Fundamental Research,
Homi Bhabha Road, Mumbai 400005, India.*

^a Electronic address: mpatil@impan.pl

^b Electronic address: pritimishra@hri.res.in

^c Electronic address: dna@tifr.res.in

ABSTRACT

Binary black holes have been in limelight off late due to the detection of gravitational waves from coalescing compact binaries in the events GW150914 and GW151226. In this paper we study gravitational lensing by the binary black holes modeled as an equal mass Majumdar-Papapetrou di-hole metric and show that this system displays features that are quite unprecedented and absent in any other lensing configuration investigated so far in the literature. We restrict our attention to the light rays which move on the plane midway between the two identical black holes, which allows us to employ various techniques developed for the equatorial lensing in the spherically symmetric spacetimes. If distance between the two black holes is below a certain threshold value, then the system admits two photon spheres. As in the case of single black hole, infinitely many relativistic images are formed due to the light rays which turn back from the region outside the outer (unstable) photon sphere, all of which lie beyond a critical angular radius with respect to the lens. However in the presence of the inner (stable) photon sphere, the effective potential now turns upwards again and the light rays that enter the outer photon sphere can turn back, leading to the formation of a new set of infinitely many relativistic images, all of which lie below the critical radius from the lens mentioned above. As the distance between the two black hole is increased, two photon spheres approach one another, merge and eventually disappear. In the absence of the photon sphere, apart from the formation of a finite number of discrete relativistic images, the system remarkably admits a radial caustic, which has never been observed in the context of relativistic lensing before. Thus the system of binary black hole admits novel features both in the presence and absence of photon spheres. We discuss possible observational signatures and implications of the binary black hole lensing.

I. INTRODUCTION

The first detection of gravitational waves was made recently by Advanced LIGO on September 14, 2015 validating the Einstein's general theory of relativity [1]. It was soon followed by the second detection on December 26, 2015. These events are referred to as GW150914 and GW151226 [2]. In both the events the gravitational waves were generated by a pair of black holes which orbited one another with decaying orbits and eventually merged to form a single black hole. A gigantic amount of energy worth 3 solar masses was emitted in the first event GW150914 within the timescale of few milli-seconds exceeding the integrated intensity of all stars in the observable universe by two orders of magnitude. These and many other observations related to binary black holes in electromagnetic band [3],[4] suggest that the system consisting of two black holes in the close vicinity can host a wide variety of remarkable phenomenon that would be interesting both from the point of view of astrophysics and fundamental physics. In this paper we explore binary black holes from a different perspective. We study gravitational lensing by a pair of black holes and show that this system can exhibit novel features which are quite unprecedented and absent in any other gravitational lensing configuration studied so far.

The two body problem in general relativity is extremely difficult, in contrast with Newtonian gravity. This is essentially consequence of the fact that Einstein equations are complicated coupled non-linear partial differential equations that are difficult to deal with. There are no exact solutions to Einstein equations depicting binary black holes that could be applicable in the realistic astrophysical context. In this paper we work with the Majumdar-Papapetrou solution depicting multiple black holes in the equilibrium, which could be thought of as a simple toy model that might capture some of the features in a realistic scenario. Majumdar-Papapetrou metric is perhaps the simplest multi-black hole solution known so far. It was discovered independently by Majumdar and Papapetrou [5],[6] and later demonstrated to represent spacetime with multiple black holes [7]. There were many interesting investigations that were carried out in the context of Majumdar-Papapetrou spacetime recently [8], [9], [10], [11].

We focus on the case where Majumdar-Papapetrou metric represents two identical equal mass non-rotating black holes at rest with respect to one another at certain distance. The metric is static, has a rotational symmetry around the line joining two black holes and reflec-

tion symmetry about the plane that is midway between the two black holes, which intersects line joining two black holes orthogonally. We assume that the light source and observer are located on the symmetry plane and focus on light rays which are confined to move on this plane. This allows us to employ various techniques developed to study gravitational lensing on the equatorial plane of spherically symmetric spacetimes [12],[13],[14],[15],[16],[17]. The central point of the symmetry plane which is also the point exactly midway between two black holes on the axis essentially acts as a gravitational lens. The photon sphere plays an important role in the relativistic gravitational lensing. Recently it was demonstrated [9] that the number of photon spheres on the symmetry plane depends on the distance between the two black holes. If the distance between the two black holes is small, then the symmetry plane exhibits two photon spheres, one of which is unstable and the other one is stable. As the distance is increased the two photon spheres approach each other, merge and disappear. So when the distance is larger than the certain critical threshold value, there are no photon spheres. The properties of relativistic images and caustics are radically different depending on whether two photon spheres are present and absent.

The structure of images formed due to the photons that turn back from the region above the outer unstable photon sphere is same as in the case of Schwarzschild black hole [13],[14]. All the images lie beyond certain critical angular radius with respect to the lens. There are infinite images clubbed together close to this critical radius. In case of Schwarzschild black hole there is a dark region below the critical radius with no images, which is consequence of the fact that the light rays which enter the single unstable photon sphere never turn back and enter black hole. The situation is drastically different in case of the di-hole in the presence of second stable inner photon sphere. As we will show, the effective potential turns upward again and the photons that enter outer photon sphere can now turn back. This leads to the formation of new infinite set of relativistic images, all of which lie inside the critical radius mentioned above. The region which would have been dark in the case of a single black hole, is not dark in the presence of the two photon spheres. Again most of the images are crowded together close to the critical radius and few discrete images lie close to the lens. In the absence of the photon sphere a finite number of discrete relativistic images are formed. Interestingly the radial caustic is present in this case. This is the location where the map between image plane and source plane is degenerate. Relativistic radial caustic has never been reported before in any other investigation so far. Thus we demonstrate that new

novel features arise both in the presence and absence of twin photon spheres.

We note that the system similar to the one we investigated in this paper where there are two black holes and source which could be bright spot in the accretion disk or maybe in the gas cloud falling towards black holes may not be so hard to realize in the nature. Based on our analysis and expectation that we might capture some of the features in the realistic scenario, we anticipate that the gravitational lensing signature of such a system will be characteristic and peculiar. Thus gravitational lensing signal will allow us to locate a binary black hole system in the sky and thus reduce the number of parameters in the search for gravitational waves from binary black holes in the interferometric detectors such as LIGO, VIRGO and KAGRA using matched filtering. This suggests that our investigation could possibly have serious implications for gravitational wave data analysis.

II. MAJUMDAR-PAPAPETROU DI-HOLE METRIC AND PHOTON SPHERES

In this section we describe the Majumdar-Papapetrou di-hole metric and null geodesics. In classical mechanics a system of particles at rest with charge equal to mass is in the equilibrium for arbitrary distance between the particles. Interestingly same is true in general relativity as well. A system of maximally charged non-rotating black holes are in equilibrium irrespective of the distance between them. The static electro-vacuum spacetime depicting this scenario is Majumdar-Papapetrou metric which is the simplest multi-black hole exact solution in general relativity and thus it has served as a toy-model for numerous analytical investigations as quoted in the introductory section.

In this paper we focus on the special case of the Majumdar-Papapetrou metric which represents two equal mass maximally charged non-rotating black holes in equilibrium at fixed distance between them. We call it a di-hole metric. The spacetime is static and asymptotically flat. It admits a rotational symmetry about the line joining two black holes and reflection symmetry about the plane that is midway between the black holes. In the cylindrical coordinate system (t, ρ, ϕ, z) , which is well-adapted to the symmetries, the di-hole metric is given by

$$ds^2 = -\frac{dt^2}{U^2} + U^2(d\rho^2 + \rho^2 d\phi^2 + dz^2), \quad (1)$$

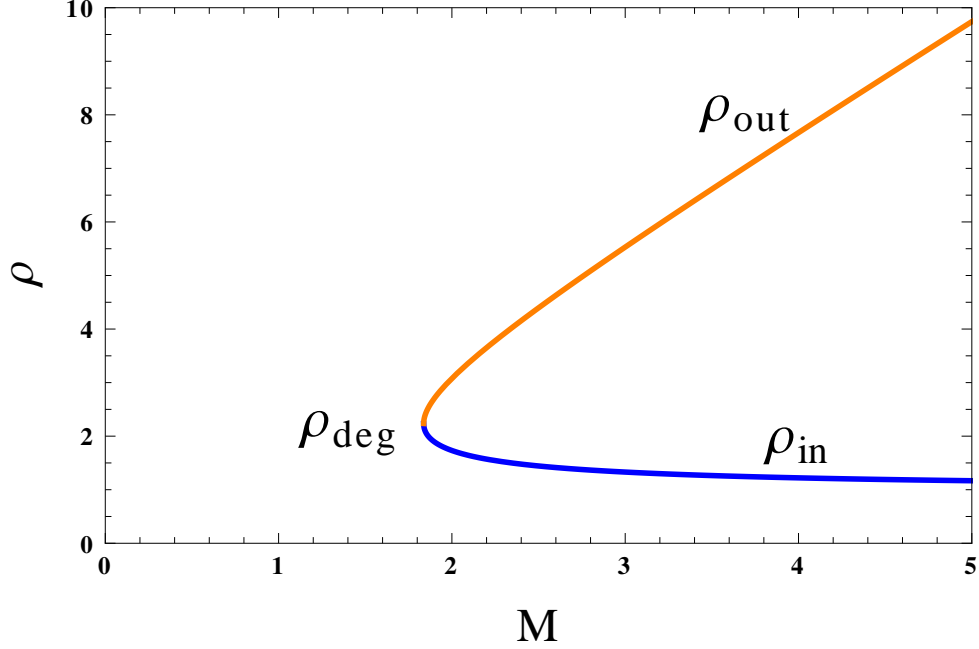


FIG. 1. The radius of photon sphere ρ is plotted against the mass to distance ratio M . Below $M = M_* = \sqrt{\frac{27}{8}}$ there is no photon sphere. At $M = M_*$ we have a single degenerate photon sphere located at $\rho_{deg} = \sqrt{5}$. Above $M > M_*$ there are two photon spheres. The radius of outer photon sphere is denoted by ρ_{out} and that of inner photon sphere is denoted by ρ_{in} .

where the metric function $U(\rho, z)$ is given by

$$U(\rho, z) = 1 + \frac{M}{\sqrt{\rho^2 + (z - a)^2}} + \frac{M}{\sqrt{\rho^2 + (z + a)^2}}. \quad (2)$$

Each of the black holes has mass M . The black holes are located at $z = +a$ and $z = -a$ on z -axis about which there is a rotational symmetry and the symmetry plane $z = 0$ is located midway between the two black holes. In this coordinates black holes appear as points. We find it to convenient to work in the units where a is set to unity and thus all dimensional quantities are appropriately expressed in units of a which is half of the coordinate distance between the two black holes.

We focus our attention on the null geodesics that are restricted to move on the symmetry plane $z = 0$. Let V be the four-velocity of the light ray. Using the standard techniques of dealing with null geodesics with the help of conserved quantities associated with symmetries of metric and normalization of velocity we obtain the non-zero components of four-velocity

as

$$\begin{aligned} V^t &= \frac{U^2}{b}, \\ V^\phi &= \pm \frac{1}{U^2 \rho^2}, \\ V^\rho &= \pm \sqrt{\frac{1}{b^2} - \frac{1}{U^4 \rho^2}}, \end{aligned} \quad (3)$$

where b is the impact parameter, \pm in the expression for V^ϕ stands for the photons moving clockwise and anti-clockwise respectively and \pm in the expression for V^ρ stands for the photons which move in radially outwards and inwards respectively. The function U in the expression above is now

$$U(\rho) = 1 + \frac{2M}{\sqrt{\rho^2 + 1}}, \quad (4)$$

where M is twice ratio of mass and distance between the black holes. The equation describing the radial motion of the light ray can be recast in the form

$$V^{\rho^2} + V_{eff}(\rho) = \frac{1}{b^2} \quad ; \quad V_{eff}(\rho) = \frac{1}{U^4 \rho^2}. \quad (5)$$

V_{eff} is the effective potential for radial motion. It is quite useful to use the analogy of a particle moving in potential well in classical mechanics while dealing with the radial motion of photon.

The location of the circular photon orbit i.e. photon sphere can be obtained by solving the equation $\frac{dV_{eff}}{d\rho} = 0$ which is given by

$$(\rho^2 + 1)^{\frac{3}{2}} = 2M (\rho^2 - 1). \quad (6)$$

With the substitution $\eta^2 = \rho^2 + 1$, the above equation can be cast into a cubic equation

$$\eta^3 - 2M\eta^2 + 4M = 0. \quad (7)$$

The existence or otherwise of the photon spheres is determined by the discriminant of the cubic $\Delta = 128M^2 (M^2 - 27/8)$. The critical value of parameter M for which discriminant is zero is given by

$$M_* = \sqrt{\frac{27}{8}}. \quad (8)$$

When $M > M_*$, the discriminant of cubic is positive and two photon spheres are present. We obtain location of the photon spheres by solving the cubic equation with Trigonometric

method. The location of the outer photon sphere denoted by ρ_{out} is given by

$$\rho_{out} = \sqrt{\frac{4M^2}{9} \left(1 + 2 \cos \left[\frac{1}{3} \cos^{-1} \left(1 - \frac{27}{4M^2} \right) \right] \right)^2 - 1}. \quad (9)$$

The effective potential V_{eff} admits a maximum at $\rho = \rho_{out}$ and hence the outer photon sphere is "unstable". The location of inner photon sphere denoted by ρ_{in} is given by

$$\rho_{in} = \sqrt{\frac{4M^2}{9} \left(1 - 2 \sin \left[\frac{\pi}{6} - \frac{1}{3} \cos^{-1} \left(1 - \frac{27}{4M^2} \right) \right] \right)^2 - 1}. \quad (10)$$

Since the effective potential admits a minimum at $\rho = \rho_{in}$, the inner photon sphere is "stable". The location of photon spheres as a function of M is depicted in Fig.1, which is same as Fig.4 in [9].

When $M = M_*$, two photon spheres coincide and we have a single degenerate photon sphere located at

$$\rho_{deg} = \sqrt{5}. \quad (11)$$

Whereas in the case $M < M_*$, the discriminant of a cubic is negative and circular photon orbits are absent.

As mentioned earlier M is ratio of mass to the distance between the black holes. So the results obtained in this section imply that for a fixed mass, if the distance between the black holes is below certain critical value, two photon spheres are present on the symmetry plane $z = 0$ midway between the black holes. As the black holes recede from another, two photon spheres come together, merge and eventually disappear above the critical distance. As we demonstrate in this paper, the gravitational lensing signature of binary black holes is radically different depending on whether the photon spheres are present. Thus the separation between the black holes for fixed mass dictates the existence or otherwise of twin photon spheres and the gravitational lensing signature of the binary black holes.

III. GRAVITATIONAL LENSING BY THE MAJUMDAR-PAPAPETROU DI-HOLE

In this section we describe the basics of the gravitational lensing formalism that we employ in our investigation of Majumdar-Papapetrou di-hole. We assume that the source of light and observer are located on the symmetry plane $z = 0$ placed midway between the black

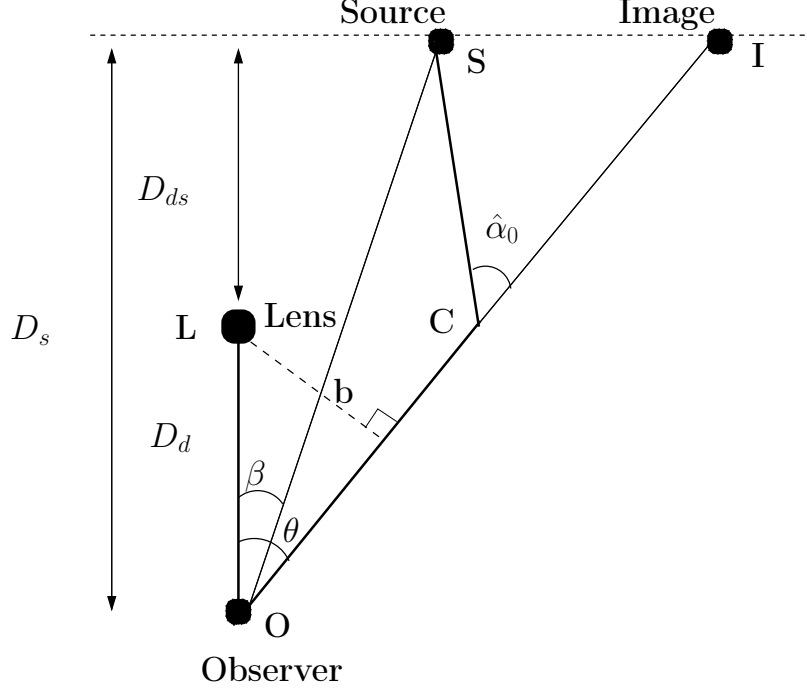


FIG. 2. The lens diagram. S , O , I and L stand for the source, observer, image and lens respectively. $\hat{\alpha}_0$ is the deflection angle. D_{ds} , D_d and D_s are lens-image, lens-observer and source-observer distances respectively. Angle β depicts the source location and θ depicts the image location. b is the impact parameter.

holes. We restrict our attention to the light rays that are allowed to move on the plane $z = 0$. This allows us to employ the formalism developed for the lensing of light on the equatorial plane of spherically symmetric spacetimes. We note that the central point with $\rho = 0$ on the plane $z = 0$, which is also the point midway between the two identical black holes, essentially acts as a gravitational lens in our investigation for all practical purposes.

We assume that both source and observer are located faraway from the central point and also from the two black holes in the asymptotic region which is approximately flat. Thus the light ray starts from infinity, falls toward the center as it gets bent, admits a turning point at $\rho = \rho_0$ and returns to infinity. The total amount of deflection suffered by the light ray in its journey is given by

$$\hat{\alpha}(\rho_0) = 2 \int_{\rho_0}^{\infty} \frac{|V^\phi|}{|V^\rho|} d\rho - \pi = 2 \int_{\rho_0}^{\infty} \frac{1}{\rho} \frac{\sqrt{V_{eff}(\rho)}}{\sqrt{V_{eff}(\rho_0) - V_{eff}(\rho)}} d\rho - \pi. \quad (12)$$

While obtaining the equation above from (3) we have used the fact that radial component

of velocity is zero at the turning point, i.e., $V^\rho(\rho_0) = 0$ and thus the impact parameter b can be related to ρ_0 via

$$b = \frac{1}{\sqrt{V_{eff}(\rho_0)}}. \quad (13)$$

Later in the paper we employ clever techniques proposed by Bozza [15] and develop their generalizations in order to get an approximate expression for deflection angle in various situations.

We further assume that the source is located approximately behind the lens with respect to the observer. This allows us to use Virbhadra-Ellis lens equation [13]. We note that there are other lens equations in the literature which also work equally well in this approximation such as Virbhadra-Narasimha-Chitre lens equation proposed earlier in [12] and so on.

The lens diagram is depicted in Fig.2. L in the diagram is the lens which is central point of $z = 0$ plane in this context. The observer is located at O . The line joining observer and lens is optic axis. S is the location of source which is almost exactly behind the lens with respect to observer. The source is located at an angle β with respect to optic axis as seen by the observer. The light ray which initially travels along line SC gets bent in the vicinity of the lens and arrives at the observer moving along CO . Thus to the observer the light seems to originate from I which is the perceived image. The image is located at angle θ with respect to the optic axis. The deflection suffered by the light ray on its journey from source to the observer is $\hat{\alpha}_0$. The light can go around the lens multiple times. Hence the deflection angle can be very large. The distances between lens-image, lens-observer and source-observer are given by D_{ds} , D_d and D_s respectively.

The Virbhadra-Ellis lens equation allows us to relate the source location β , image location θ and the deflection angle $\hat{\alpha}_0$ and is given by

$$\tan \beta = \tan \theta - \frac{D_{ds}}{D_s} (\tan \theta + \tan (\hat{\alpha}_0 - \theta)). \quad (14)$$

Another relation that we can write down from the lens diagram is

$$\sin \theta = \frac{b}{D_d}. \quad (15)$$

From Eqs.(12),(13),(14) we can write deflection angle $\hat{\alpha}_0$ in terms of θ and then use lens equation Eq.(14) to solve for the image locations θ for a given source location β . Solving lens equation is not so easy as it is a complicated transcendental equation. One has to often resort to numerical techniques. Analytical way of solving lens equation in certain situations

was proposed by Bozza in [15] which we generalize and develop further in this paper. For this we use the fact that the source is almost exactly behind the source and thus angles β and α are small and deviation of deflection angle from multiple of 2π is very small, i.e.,

$$\hat{\alpha}_0 = 2\pi n + \delta\alpha_n \quad ; \quad |\delta\alpha_n| \ll 1. \quad (16)$$

This allows us to simplify lens equation Eq.(14) and Eq.(15) as

$$\beta = \theta - \frac{D_{ds}}{D_s} \delta\alpha_n, \quad (17)$$

and

$$\theta = \frac{b}{D_d}. \quad (18)$$

We will employ these equations later in the paper.

The lens equation allows us to relate image location to the source location and set up a map from image plane to source plane. A radial caustic is admitted if this map is degenerate, i.e.

$$\frac{d\beta}{d\theta} = 0. \quad (19)$$

We now derive an expression for $\frac{d\beta}{d\theta}$. From Eq.(14), we get

$$\frac{d\beta}{d\theta} = \frac{\cos^2 \beta}{\cos^2 \theta} \left[1 - \frac{D_{ds}}{D_s} \left\{ 1 + \frac{\cos^2 \theta}{\cos^2(\hat{\alpha}_0 - \theta)} \left(\frac{d\hat{\alpha}_0}{d\rho_0} \frac{d\rho_0}{d\theta} - 1 \right) \right\} \right], \quad (20)$$

where $\frac{d\rho_0}{d\theta}$ and $\frac{d\hat{\alpha}_0}{d\rho_0}$ are as given below. From Eqs.(13),(15) we get

$$\frac{d\rho_0}{d\theta} = -2 \frac{V_{eff}(\rho_0)}{V'_{eff}(\rho_0)} \sqrt{D_d^2 V_{eff}(\rho_0) - 1}, \quad (21)$$

and from Eq.(12) after implementing few clever tricks we get

$$\frac{d\hat{\alpha}_0}{d\rho_0} = 2 \int_{\rho_0}^{\infty} \left[\frac{1}{\sqrt{V_{eff}(\rho_0) - V_{eff}(\rho)}} \frac{d}{d\rho} \left(\frac{\sqrt{V_{eff}(\rho)}}{\rho} \right) - \frac{1}{2} \frac{\sqrt{V_{eff}(\rho)} (V'_{eff}(\rho_0) - V'_{eff}(\rho))}{\rho (V_{eff}(\rho_0) - V_{eff}(\rho))^{\frac{3}{2}}} \right] d\rho, \quad (22)$$

where prime denotes the derivative with respect to ρ . Radial caustic occurs when two images for a given source location coincide, has never been reported so far in the context of relativistic gravitational lensing. We will show that the radial caustic is admitted in the absence of the photon sphere, when the distance between two black holes is larger than a critical threshold value in Majumdar-Papapetrou di-hole spacetime.

Whenever required, for numerical computation we choose the following set of convenient parameters. We assume that the source and observer are equidistant from the lens. The mass of each of the black hole in binary is taken to be same as the mass of the galactic central supermassive black hole in Milky way which is $2.8 \times 10^6 M_\odot$ and also we take distance of observer from lens to be same as the distance of earth from central supermassive black hole, i.e. 8.5kpc. The angular location of source is taken to be $\beta = 0.075$ radian.

Three cases $M > M_*$, $M = M_*$ and $M < M_*$ when two photon spheres are present, when a single degenerate photon sphere is present and when no photon spheres are present respectively require separate consideration and analysis and thus they are dealt with independently in the subsequent sections. Our aim is to analyze the structure of images and existence of caustic in the near-aligned configuration of source, lens and observer.

IV. TWO PHOTON SPHERES

In this section we focus our attention on the case $M > M_*$ when two photon spheres are present on the symmetry plane $z = 0$ centered at $\rho = 0$. The locations of the outer unstable photon sphere ρ_{out} and inner stable photon sphere ρ_{in} are given by Eqs.(9),(10). The effective potential admits maximum at $\rho = \rho_{out}$ and minimum at $\rho = \rho_{in}$ as shown in Fig.3. For lower values of ρ , the effective potential rises upwards below the inner photon sphere. $\rho = \rho_1$ is a point such that the effective potential at this location is same as the effective potential at maximum, i.e. $V_{eff}(\rho_1) = V_{eff}(\rho_{out})$. The light rays for which $b > 1/\sqrt{V_{eff}(\rho_{out})}$ turn back from $\rho_0 > \rho_{out}$. Whereas the light rays for which $b < 1/\sqrt{V_{eff}(\rho_{out})}$, enter outer photon sphere and admit turning point below $\rho = \rho_1$, i.e. $\rho_0 < \rho_1$. This situation is quite different in case of the black holes where the effective potential does not rise again for lower values of radial coordinates and light rays which enter the photon sphere necessarily enter the event horizon. Thus new relativistic images are formed due to the lights rays which turn back in the region below outer photon sphere in dihole spacetime which are absent in black hole case.

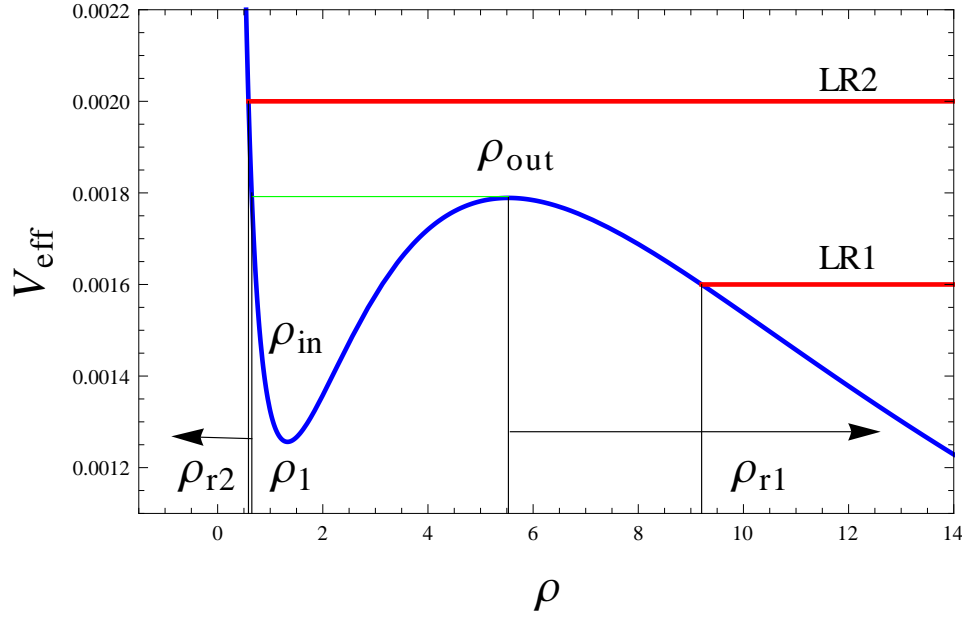


FIG. 3. The effective potential V_{eff} is plotted as a function of ρ for $M = 3 > M_*$ denoted by blue curve. It admits a maximum at $\rho = \rho_{out}$ and a minimum at $\rho = \rho_{in}$. As shown in the figure effective potential rises again below the inner photon sphere for the smaller values of ρ . At $\rho = \rho_1$, we have $V_{eff}(\rho_1) = V_{\rho_{out}}$ i.e. the value of the effective potential is same as that at maximum. When $b > 1/\sqrt{V_{eff}(\rho_{out})}$, light rays turn back from the region outside the outer photon sphere denoted by arrow which points towards right. Such a light ray depicted by $LR1$ which turns back from $\rho = \rho_{r1} > \rho_{out}$. Whereas the light rays with $b < 1/\sqrt{V_{eff}(\rho_{out})}$ turn back from the region below $\rho = \rho_1$ denoted by arrow which points towards left. Such a light ray is denoted by $LR2$ which enters the outer photon sphere and turns back from $\rho = \rho_{r2} < \rho_1$.

A. Images due to the light rays that turn back outside outer photon sphere.

Initially we focus on the light rays that admit turning point at $\rho = \rho_0$ outside the outer photon sphere and calculate the location of the images formed. Further we assume that the deflection point is in fact very close to the photon sphere. This greatly simplifies the discussion and allows us to do calculations analytically.

We find it convenient to introduce new radial coordinate y following the discussion in [15]

which is related to the old coordinate ρ by

$$y = \frac{\left(\frac{1}{U(\rho)} - \frac{1}{U(\rho_0)}\right)}{\left(1 - \frac{1}{U(\rho_0)}\right)}. \quad (23)$$

U is a monotonically decreasing function. Thus it follows that y increases monotonically from 0 to 1 as ρ varies from ρ_0 to ∞ . It is also useful to invert the relation above and write ρ in terms of y as

$$\rho(y) = U^{-1} \left(\frac{U(\rho_0)}{U(\rho_0) + 1 - y} \right), \quad (24)$$

where U^{-1} is an inverse function of U . We define a function $T(\rho_0, \rho)$ as

$$T(\rho_0, \rho) = \frac{d\rho}{dy} = -\frac{U(\rho)^2}{U'(\rho)} \left(1 - \frac{1}{U(\rho_0)} \right). \quad (25)$$

The deflection angle $\hat{\alpha}_0$ can be written as

$$\hat{\alpha}_0 = I - \pi. \quad (26)$$

I in the expression above is

$$I = \int_{\rho_0}^{\infty} \frac{2}{\rho} \frac{\sqrt{V_{eff}(\rho)}}{\sqrt{V_{eff}(\rho_0) - V_{eff}(\rho)}} d\rho = \int_0^1 \frac{F(\rho_0, \rho(y))}{\sqrt{V_{eff}(\rho_0) - V_{eff}(\rho(y))}} dy, \quad (27)$$

where $F(\rho_0, \rho(y))$ is a function given by

$$F(\rho_0, \rho(y)) = \frac{2}{\rho} \sqrt{V_{eff}(\rho(y))} T(\rho_0, \rho(y)). \quad (28)$$

The function $F(\rho_0, \rho(y))$ is finite and well-behaved for all values of $y \in (0, 1)$. Whereas $1/\sqrt{V_{eff}(\rho_0) - V_{eff}(\rho(y))}$ diverges at $y = 0$. Taylor expanding $(V_{eff}(\rho_0) - V_{eff}(\rho(y)))$ around $y = 0$, we get

$$V_{eff}(\rho_0) - V_{eff}(\rho(y)) = \alpha_1(\rho_0)y + \beta_2(\rho_0)y^2 + O(y^3), \quad (29)$$

where $\alpha_1(\rho_0)$ and $\beta_1(\rho_0)$ are given by

$$\begin{aligned} \beta_1(\rho_0) &= -\frac{1}{2} \left(T^2(\rho_0, \rho = \rho_0) V_{eff}''(\rho_0) + T(\rho_0, \rho = \rho_0) T'(\rho_0, \rho = \rho_0) V_{eff}'(\rho_0) \right), \\ \alpha_1(\rho_0) &= -F(\rho_0, \rho = \rho_0) V_{eff}'(\rho_0). \end{aligned} \quad (30)$$

When turning point $\rho = \rho_0$ is away from the outer photon sphere $\rho = \rho_{out}$, $\alpha_1(\rho_0)$ is a non-zero positive finite number. Thus the integral Eq(27) and the deflection suffered by the light ray is finite.

The situation is quite different when the turning point is close to the outer photon sphere. We expand $\alpha_1(\rho_0)$ and $\beta_1(\rho_0)$ around $\rho_0 = \rho_{out}$ and get

$$\begin{aligned}\beta_1(\rho_0) &= -\frac{1}{2}T^2(\rho_{out}, \rho = \rho_{out})V''_{eff}(\rho_{out}) + O(\rho_0 - \rho_{out}), \\ \alpha_1(\rho_0) &= \frac{2\beta_1(\rho_{out})}{T(\rho_{out}, \rho = \rho_{out})}(\rho_0 - \rho_{out}) + O((\rho_0 - \rho_{out})^2).\end{aligned}\quad (31)$$

To the leading order $\alpha_1(\rho_0)$ is vanishingly small and thus the integral Eq(27) and the deflection angle show divergence. We isolate the divergence piece in the integral Eq(27) as

$$I_{1D}(\rho_0) = F(\rho_{out}, \rho = \rho_{out}) \int_0^1 \frac{1}{\sqrt{\alpha_1(\rho_0)y + \beta_2(\rho_0)y^2}} dy = -A_1 \log\left(\frac{\rho_0}{\rho_{out}} - 1\right) + \tilde{B}_1 + O(\rho_0 - \rho_{out}), \quad (32)$$

where

$$\begin{aligned}A_1 &= \frac{F(\rho_{out}, \rho = \rho_{out})}{\sqrt{\beta_1(\rho_{out})}}, \\ \tilde{B}_1 &= \frac{F(\rho_{out}, \rho = \rho_{out})}{\sqrt{\beta_1(\rho_{out})}} \log\left(\frac{2T(\rho_{out}, \rho = \rho_{out})}{\rho_{out}}\right),\end{aligned}\quad (33)$$

and the regular piece in the integral can be written as

$$I_{1R}(\rho_0) = \int_0^1 \left(\frac{F(\rho_0, \rho(y))}{\sqrt{V_{eff}(\rho_0) - V_{eff}(\rho(y))}} - \frac{F(\rho_{out}, \rho = \rho_{out})}{\sqrt{\alpha_1(\rho_0)y + \beta_2(\rho_0)y^2}} \right) dy = I_{1R}(\rho_{out}) + O(\rho_0 - \rho_{out}). \quad (34)$$

Combining divergent part $I_{1D}(\rho_0)$ and regular parts of the integral $I_{1R}(\rho_0)$, we can write down the deflection angle $\hat{\alpha}_0$ as

$$\hat{\alpha}_0 = -A_1 \log\left[B_1 \left(\frac{\rho_0}{\rho_{out}} - 1\right)\right] - \pi + O((\rho_0 - \rho_{out})^2), \quad (35)$$

where B_1 is related to \tilde{B}_1 , A_1 and $I_{1R}(\rho_{out})$ by

$$B_1 = \exp\left(-\frac{\tilde{B}_1 + I_{1R}(\rho_{out})}{A_1}\right). \quad (36)$$

Thus the deflection angle shows logarithmic divergence as the reflection point approaches the outer photon sphere.

The impact parameter b upon expansion around the outer photon sphere can be written as

$$b = C_1 + D_1 \left(\frac{\rho_0}{\rho_{out}} - 1\right)^2 + O((\rho_0 - \rho_{out})^3), \quad (37)$$

where C_1 and D_1 are given by

$$\begin{aligned} C_1 &= \frac{1}{\sqrt{V_{eff}(\rho_{out})}}, \\ D_1 &= -\frac{1}{2} \frac{V_{eff}''(\rho_{out})}{V_{eff}^{\frac{3}{2}}(\rho_{out})} \rho_{out}^2. \end{aligned} \quad (38)$$

Using Eqs.(18),(35),(37) we can relate θ to the deflection angle as

$$\theta = \frac{C_1}{D_d} + \frac{D_1}{D_d} \frac{1}{B_1^2} \exp\left(-\frac{2}{A_1}(\hat{\alpha}_0 + \pi)\right), \quad (39)$$

and using Eqs.(16),(17),(39) we can compute locations of images $\theta_{1,n}$ for a given source location β in the near-aligned configuration, which are given by

$$\theta_{1,n} = \frac{C_1}{D_d} + \frac{D_1}{D_d} \frac{1}{B_1^2} \exp\left(-\frac{2}{A_1}(2n+1)\pi\right) \left(1 + \frac{2}{A_1} \frac{D_s}{D_{ds}} \beta\right). \quad (40)$$

Here n stands for the number of times light ray goes around the lens during its journey from source to observer. It turns out that all the images lie beyond a certain critical angle $\bar{\theta}_1$ given by

$$\bar{\theta}_1 = \frac{C_1}{D_d}. \quad (41)$$

As n increases images get closer and closer to the critical angle $\bar{\theta}_1$ and asymptotically approach it from right. So far we dealt with the light rays which go around the lens in the clockwise sense. For the light rays which go around the lens in counter-clockwise sense the images occur on the opposite side of the optic axis and their locations $\theta'_{1,n}$ are given by

$$\theta'_{1,n} = -\frac{C_1}{D_d} + \frac{D_1}{D_d} \frac{1}{B_1^2} \exp\left(-\frac{2}{A_1}(2n+1)\pi\right) \left(-1 + \frac{2}{A_1} \frac{D_s}{D_{ds}} \beta\right). \quad (42)$$

The pattern of the images formed due to the single black hole is qualitatively similar to the images formed in case of the di-hole due to the light rays that are reflected back outside the outer photon sphere. In case of the black hole there is a dark region below the critical radius as there are no images formed in this region. As we show in this paper that is not the case for di-hole as the light rays which turn back from the region inside photon sphere form new images filling in the void.

B. Images formed due to the light rays that turn back inside the photon sphere.

We now compute the pattern of images formed due to the light rays that enter the outer photon sphere and turn back at the radial coordinate $\rho_0 < \rho_1$ and reach infinity again. As

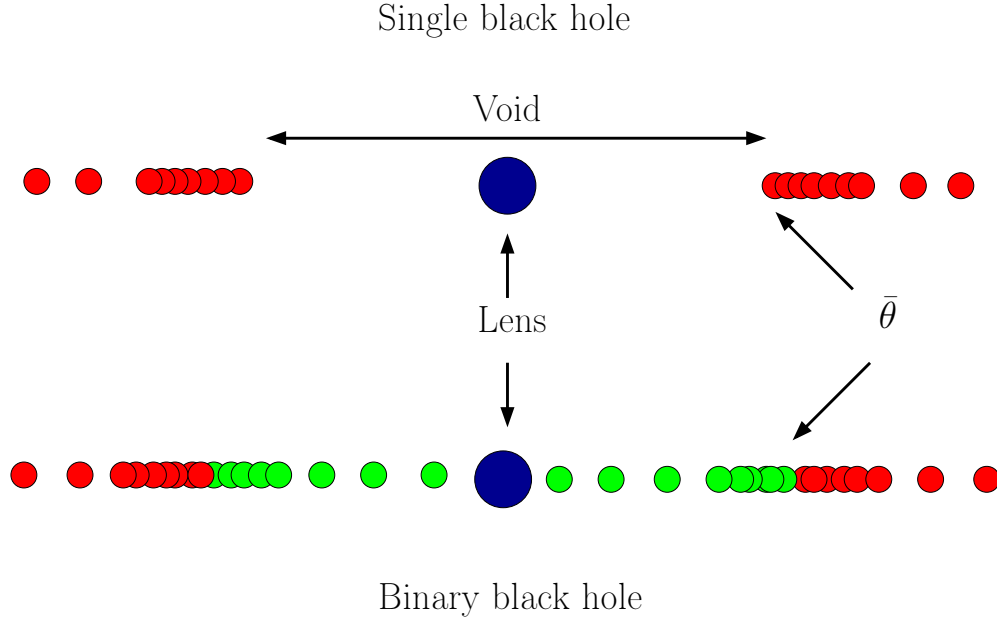


FIG. 4. Pattern of images in the case of single black hole (upper panel) and binary black hole (lower panel). In case of the single black hole images are formed due to the light rays that turn back outside the photon sphere and lie beyond critical angle $\bar{\theta}$ with respect to the lens. There is a dark region below the critical angle denoted as "Void" in the figure where no images are formed. In case of the binary black hole there are two photon spheres when $M > M_*$ and light rays which enter photon sphere can turn back and hence we get new images. Red dots in the lower panel are images formed due to the light rays which turn back outside the outer photon sphere and lie beyond the critical angle $\bar{\theta}$. Whereas the green dots represent the images formed due to the light rays which admit turning point inside the photon sphere, all of which lie below the critical angle $\bar{\theta}$. Thus a new set of relativistic images fills in the void present in case of the single black hole and illuminate the dark region.

mentioned earlier ρ_1 is a location such that

$$V_{eff}(\rho_1) = V_{eff}(\rho_{out}). \quad (43)$$

We use the coordinate y introduced earlier Eq.(23). The deflection angle can be written as before in Eqs.(26),(27)

$$\hat{\alpha}_0 = I - \pi = \int_0^1 \frac{F(\rho_0, \rho(y))}{\sqrt{V_{eff}(\rho_0) - V_{eff}(\rho(y))}} dy - \pi. \quad (44)$$

$F(\rho_0, \rho(y))$ is finite and well-behaved everywhere. On the other hand $1/\sqrt{V_{eff}(\rho_0) - V_{eff}(\rho(y))}$ diverges when $y = 0$ i.e. at $\rho = \rho_0$ and at $\rho = \rho_{out}$ i.e. $y = y_{out}$ when ρ_0 is close to ρ_1 . Here y_{out} is given by $y_{out} = (1/U(\rho_{out}) - 1/U(\rho_0))/(1 - 1/U(\rho_0))$.

We first focus on $\rho = \rho_0$ and expand $V_{eff}(\rho_0) - V_{eff}(\rho(y))$ around $y = 0$. To the leading order we obtain

$$V_{eff}(\rho_0) - V_{eff}(\rho(y)) = \alpha_2(\rho_0)y + O(y^2), \quad (45)$$

where $\alpha_2(\rho_0)$ is given by

$$\alpha_2(\rho_0) = -T'(\rho_0, \rho = \rho_0)V_{eff}'(\rho_0). \quad (46)$$

Since $\alpha_2(\rho_0)$ is a finite, positive non-zero number, divergent behavior of integrand can be tamed when we compute the integral I and it does not result in the divergent behavior of deflection angle.

We now focus on $\rho = \rho_{out}$ and expand $V_{eff}(\rho_0) - V_{eff}(\rho(y))$ around $y = y_{out}$. We get

$$V_{eff}(\rho_0) - V_{eff}(\rho(y)) = \alpha_3(\rho_{out}) + \beta_3(\rho_{out})(y - y_{out})^2 + O((y - y_{out})^3), \quad (47)$$

where $\alpha_3(\rho_{out})$ and $\beta_3(\rho_{out})$ are given by

$$\begin{aligned} \alpha_3(\rho_{out}) &= V_{eff}(\rho_0) - V_{eff}(\rho_{out}) = -V_{eff}'(\rho_1)(\rho_1 - \rho_0) + O((\rho_1 - \rho_0)^2), \\ \beta_3(\rho_{out}) &= -\frac{1}{2}T^2(\rho_1, \rho = \rho_{out})V_{eff}''(\rho_{out}) + O(\rho_0 - \rho_1). \end{aligned} \quad (48)$$

We used Eq.(43) to derive the expression above. When ρ_0 is very close to ρ_1 , integral I is divergent and so is the deflection angle $\hat{\alpha}_0$.

We identify the divergent piece in the integral I_{2D} as

$$I_{2D} = F(\rho_1, \rho = \rho_{out}) \int_0^1 \frac{1}{\sqrt{\alpha_3(\rho_0) + \beta_3(\rho_0)(y - y_{out})^2}} dy = -A_2 \log \left(1 - \frac{\rho_0}{\rho_1} \right) + \tilde{B}_2 + O(\rho_0 - \rho_{out}), \quad (49)$$

where

$$\begin{aligned} A_2 &= \frac{F(\rho_1, \rho = \rho_{out})}{\sqrt{\beta_3}}, \\ \tilde{B}_2 &= \frac{F(\rho_1, \rho = \rho_{out})}{\sqrt{\beta_3}} \log \left(\frac{4y_{out}(1 - y_{out})\beta_3}{-V_{eff}'(\rho_1)\rho_1} \right), \end{aligned} \quad (50)$$

and the regular piece in the integral I_{2R} can be written as

$$I_{2R}(\rho_0) = \int_0^1 \left(\frac{F(\rho_0, \rho(y))}{\sqrt{V_{eff}(\rho_0) - V_{eff}(\rho(y))}} - \frac{F(\rho_1, \rho = \rho_{out})}{\sqrt{\alpha_3 + \beta_3(y - y_{out})^2}} \right) dy = I_{2R}(\rho_1) + O(\rho_1 - \rho_0). \quad (51)$$

While writing the equations above we set $\rho_0 = \rho_1$ in the expression for y_{out} since $y_{out}(\rho_0) = y_{out}(\rho_1) + O(\rho_1 - \rho_0)$ and hence the error involved is at higher order. Combining the divergent piece I_{2D} and regular piece I_{2R} in the integral we can write the deflection angle $\hat{\alpha}_0$ as

$$\hat{\alpha}_0 = -A_2 \log \left(B_2 \left(1 - \frac{\rho_0}{\rho_1} \right) \right) - \pi + O(\rho_0 - \rho_{out}), \quad (52)$$

where

$$B_2 = \exp \left(-\frac{\tilde{B}_2 + I_{2R}(\rho_1)}{A_2} \right). \quad (53)$$

The deflection angle again shows the logarithmic divergence as the reflection point ρ_0 approaches ρ_1 . We now write the impact parameter b , expanding it around $\rho = \rho_1$. We get

$$b = C_2 - D_2 \left(1 - \frac{\rho_1}{\rho_0} \right) + O((\rho_0 - \rho_1)^2), \quad (54)$$

where C_2 and D_2 are given by

$$\begin{aligned} C_2 &= \frac{1}{\sqrt{V_{eff}(\rho_1)}} \\ D_2 &= -\frac{1}{2} \frac{V'_{eff}(\rho_1)}{V_{eff}^{\frac{3}{2}}(\rho_1)} \rho_1. \end{aligned} \quad (55)$$

Using Eqs.(18),(52),(54) we can relate θ to the deflection angle $\hat{\alpha}_0$ as

$$\theta = \frac{C_2}{D_d} + \frac{D_2}{D_d} \frac{1}{B_2} \exp \left(-\frac{1}{A_2} (\hat{\alpha}_0 + \pi) \right), \quad (56)$$

and using Eqs.(16),(17),(56) we can compute locations of images $\theta_{2,n}$ for a given source location β in the near-aligned configuration, which are given by

$$\theta_{2,n} = \frac{C_2}{D_d} - \frac{D_2}{D_d} \frac{1}{B_2^2} \exp \left(-\frac{1}{A_2} (2n+1)\pi \right) \left(1 + \frac{1}{A_2} \frac{D_s}{D_{ds}} \beta \right). \quad (57)$$

All the images lie below the critical angle $\bar{\theta}_2$ which is given by

$$\bar{\theta}_2 = \frac{C_2}{D_d}. \quad (58)$$

As we increase n , images get closer and closer to critical angle and asymptotically approach it from left. From Eqs.(38),(41),(43),(55),(58), we see that

$$\bar{\theta}_1 = \bar{\theta}_2. \quad (59)$$

This implies that the second set of images formed due to the light rays which enter photon sphere and turn back fill in what would have been a void and dark region in case of the single black hole below critical angle towards optic axis.

Here $\theta_{2,n}$ denote the location of images formed on the right side of the optic axis due to the light rays that move around the lens in the clockwise sense. The location of images formed on the left side of the optic axis due to the light rays which move in anti-clockwise sense are given by

$$\theta'_{2,n} = -\frac{C_2}{D_d} + \frac{D_2}{D_d} \frac{1}{B_2^2} \exp\left(-\frac{1}{A_2}(2n+1)\pi\right) \left(1 - \frac{1}{A_2} \frac{D_s}{D_{ds}} \beta\right). \quad (60)$$

We note that $I_{1R}(\rho_{out})$ and $I_{2R}(\rho_1)$ must be computed numerically since the integrals Eqs.(34),(51) are difficult to evaluate analytically. It might also be necessary to compute ρ_1 numerically since one needs to solve transcendental equation $V_{eff}(\rho_1) = V_{eff}(\rho_{out})$. All other calculations presented above can be carried out analytically.

The pattern of images formed is shown in Fig.(4). The images on the right side of the optic axis i.e. lens are associated with the light rays that move clockwise and images on the left side are associated with the light rays which move in the counter-clockwise sense. In case of a single black hole light rays which enter the photon sphere are doomed to enter the black hole. Thus images are formed due to the light rays that turn back outside the photon sphere. All images occur above the critical angle $\bar{\theta}$ and infinitely many images are clubbed together just above the critical angle as shown in the figure. No images are formed below the critical angle towards the lens resulting in the dark void. In case of the binary black hole due to the presence of inner stable photon sphere inside the outer unstable photon sphere effective potential turns upwards again and light rays which enter the outer photon sphere can turn back giving rise to another set of new relativistic images. The new images lie below the critical angle $\bar{\theta}$ as shown in the figure. Infinitely many images clubbed just below $\bar{\theta}$. Thus the region which would have been dark void is filled up with images and turns bright again. Thus the pattern of images is qualitatively different in the binary black holes spacetime.

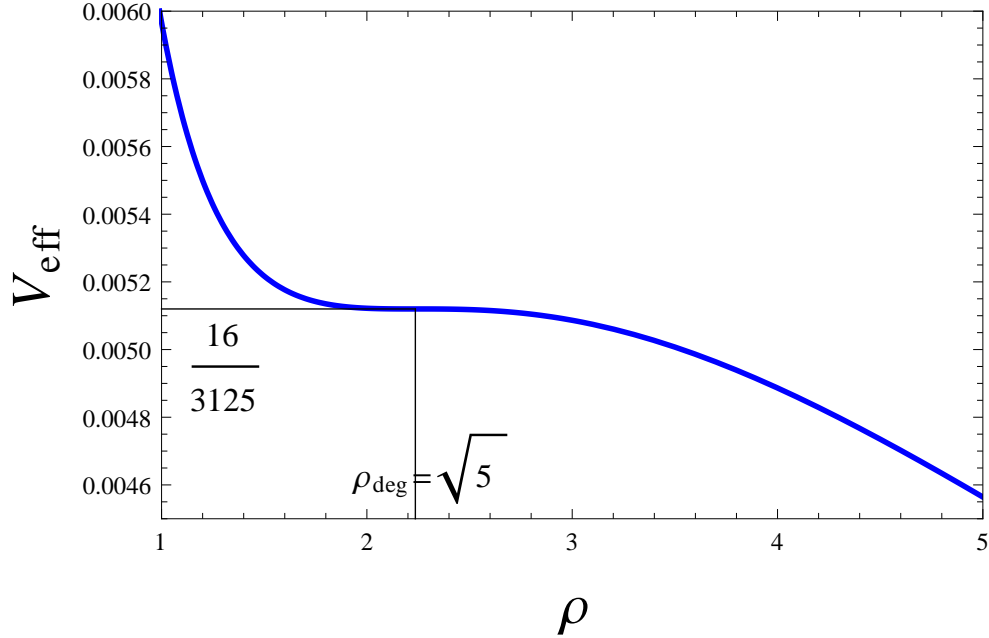


FIG. 5. Effective potential V_{eff} is plotted against ρ for the critical value of the parameter $M = M_* = \sqrt{27/8}$. The two photon spheres coincide and we have a single photon sphere located at $\rho = \rho_{deg} = \sqrt{5}$. The value of the effective potential at the location of the degenerate photon sphere is $V_{eff}(\rho_{deg}) = 16/3125$ as shown in the figure. Both first as well as second derivatives are zero at the location of photon sphere, i.e., $V'_{eff}(\rho_{deg}) = V''_{eff}(\rho_{deg}) = 0$.

V. A SINGLE DEGENERATE PHOTON SPHERE

We now deal with the case where the parameter M assumes the critical value $M = M_* = \sqrt{27/8}$. The two photon spheres we encountered in the earlier section when $M > M_*$ now coincide and we have a single degenerate photon sphere present at $\rho = \rho_{deg} = \sqrt{5}$, where both the first and second derivative of the effective potential vanish, i.e., $V'_{eff}(\rho_{deg}) = V''_{eff}(\rho_{deg}) = 0$. The value of the effective potential at the location of the degenerate photon sphere is given by $V_{eff}(\rho_{deg}) = 16/3125$. The light rays admit turning point at $\rho > \rho_{deg}$ when the impact parameter satisfies $b > 1/\sqrt{V_{eff}(\rho_{deg})}$ and at $\rho < \rho_{deg}$ when the impact parameter is $b < 1/\sqrt{V_{eff}(\rho_{deg})}$. We present here the unified treatment of the light rays that turn back both above and below the photon sphere. Such a treatment was not possible for $M > M_*$ since the light rays admitted turning points either at $\rho > \rho_{out}$ or $\rho < \rho_1$ where ρ_{out} and ρ_1 were distinct points with qualitatively different behavior of effective potential

V_{eff} .

Once again we use the new radial coordinate y with the finite range introduced in Eq.(23). The deflection angle can be written as

$$\hat{\alpha}_0 = I - \pi = \int_0^1 \frac{F(\rho, \rho(y))}{\sqrt{V_{eff}(\rho_0) - V_{eff}(\rho(y))}} dy - \pi. \quad (61)$$

We request readers to refer to section IV-A for the definition of various quantities that we use here. The function $F(\rho, \rho(y))$ is finite and well-behaved everywhere as earlier whereas $1/\sqrt{V_{eff}(\rho_0) - V_{eff}(\rho(y))}$ is divergent at $\rho = \rho_0$, i.e., at $y = 0$.

We expand $V_{eff}(\rho_0) - V_{eff}(\rho(y))$ around $y = 0$ as

$$V_{eff}(\rho_0) - V_{eff}(\rho(y)) = \alpha_4(\rho_0)y + \beta_4(\rho_0)y^2 + \gamma_4(\rho_0)y^3 + O(y^4), \quad (62)$$

where

$$\begin{aligned} \alpha_4(\rho_0) &= -T(\rho_0, \rho = \rho_0)V'_{eff}(\rho_0), \\ \beta_4(\rho_0) &= -\frac{1}{2} \left(T(\rho_0, \rho = \rho_0)T'(\rho_0, \rho = \rho_0)V'_{eff}(\rho_0) + T^2(\rho_0, \rho = \rho_0)V''_{eff}(\rho_0) \right), \\ \gamma_4(\rho_0) &= -\frac{1}{6} \left(T(\rho_0, \rho = \rho_0)T'^2(\rho_0, \rho = \rho_0)V'_{eff}(\rho_0) + T^2(\rho_0, \rho = \rho_0)T''(\rho_0, \rho = \rho_0)V'_{eff}(\rho_0) \right) \\ &\quad - \frac{1}{6} \left(3T^2(\rho_0, \rho = \rho_0)T'(\rho_0, \rho = \rho_0)V''_{eff}(\rho_0) + T^2(\rho_0, \rho = \rho_0)V'''_{eff}(\rho_0) \right) \end{aligned} \quad (64)$$

If ρ_0 is away from the photon sphere radius $\rho = \rho_{deg}$ then $\alpha_4(\rho_0)$ is finite and the integral I and deflection angle $\hat{\alpha}_0$ would be finite. If ρ_0 is reasonably close to $\rho = \rho_{deg}$ then $\alpha_4(\rho_0)$ is small but the $\beta_4(\rho_0)$ is finite when $V'_{eff}(\rho_0)$ is close to zero, however $V''_{eff}(\rho_0)$ is finite. In this intermediate region the integral I and the deflection angle $\hat{\alpha}_0$ would diverge logarithmically. In this case the calculations would be identical to that in Section IV-A.

When ρ_0 is sufficiently close to $\rho = \rho_{deg}$ both $V'_{eff}(\rho_0)$ and $V''_{eff}(\rho_0)$ take values which are close to zero. Expanding around $\rho_0 = \rho_{deg}$, we get

$$\begin{aligned} \gamma_4(\rho_0) &= -\frac{1}{6}T^3(\rho_{deg}, \rho = \rho_{deg})V'''_{eff}(\rho_{deg}) + O(\rho_0 - \rho_{deg}), \\ \alpha_4(\rho_0) &= \frac{3}{T^2(\rho_{deg}, \rho = \rho_{deg})}\gamma_4(\rho_{deg})(\rho_0 - \rho_{deg})^2 + O((\rho_0 - \rho_{deg})^3), \\ \beta_4(\rho_0) &= \frac{3}{T(\rho_{deg}, \rho = \rho_{deg})}\gamma_4(\rho_{deg})(\rho_0 - \rho_{deg}) + O((\rho_0 - \rho_{deg})^2). \end{aligned} \quad (65)$$

Since $\alpha_4(\rho_0)$ and $\beta_4(\rho_0)$ tend to zero near $\rho_0 = \rho_{deg}$, the integral I and the deflection angle $\hat{\alpha}_0$ show divergence. We extract the divergent part in the integral I as

$$I_{3D} = F(\rho_{deg}, \rho = \rho_{deg}) \int_0^1 dy \frac{1}{\sqrt{\alpha_4(\rho_0)y + \beta_4(\rho_0)y^2 + \gamma_4(\rho_0)y^3}}, \quad (66)$$

which can be written as

$$I_{3D} = \frac{A_{3,\pm}}{\sqrt{|1 - \frac{\rho_0}{\rho_{deg}}|}} + \tilde{B}_{3D}, \quad (67)$$

where $A_{3,\pm}$ and \tilde{B}_{3D} are given by

$$\begin{aligned} A_{3,\pm} &= \frac{2F(\rho_{deg}, \rho = \rho_{deg})}{\gamma_4(\rho_{deg})} \sqrt{T(\rho_{deg}, \rho = \rho_{deg})} \mathcal{I}_{\pm}, \\ \tilde{B}_{3D} &= -\frac{2F(\rho_{deg}, \rho = \rho_{deg})}{\gamma_4(\rho_{deg})}, \end{aligned} \quad (68)$$

with \mathcal{I}_{\pm} as

$$\mathcal{I}_{\pm} = \int_0^{\infty} d\xi \frac{1}{\sqrt{3 \pm 3\xi^2 + \xi^4}}. \quad (69)$$

The regular part of the integral I is given by

$$\begin{aligned} I_{3R}(\rho_0) &= \int_0^1 dy \left(\frac{F(\rho_0, \rho(y))}{\sqrt{V_{eff}(\rho_0) - V_{eff}(\rho(y))}} - \frac{F(\rho_{deg}, \rho = \rho_{deg})}{\sqrt{\alpha_4(\rho_0)y + \beta_4(\rho_0)y^2 + \gamma_4(\rho_0)y^3}} \right) \\ &= I_{3R}(\rho_{deg}) + O(\rho_0 - \rho_{deg}). \end{aligned} \quad (70)$$

Combining the divergent and convergent parts of the integral we can write the deflection angle as

$$\hat{\alpha}_0 = \frac{A_{3,\pm}}{\sqrt{|1 - \frac{\rho_0}{\rho_{deg}}|}} + B_3 - \pi + O(\rho_0 - \rho_{deg}), \quad (71)$$

where B_3 is given by

$$B_3 = \tilde{B}_{3D} + I_{3R}(\rho_{deg}). \quad (72)$$

The deflection angle shows the power law divergence unlike in the section IV where it diverged logarithmically.

Expanding the impact parameter b around $\rho_0 = \rho_{deg}$ we get

$$b(\rho_0) = C_3 + D_{3,\pm} \left| 1 - \frac{\rho_0}{\rho_{deg}} \right|^3 + O((\rho_0 - \rho_{deg})^4), \quad (73)$$

where

$$\begin{aligned} C_3 &= \frac{1}{V_{eff}(\rho_{deg})}, \\ D_{3,\pm} &= \mp \frac{1}{12} \frac{V_{eff}'''(\rho_{deg})}{V_{eff}^{\frac{3}{2}}(\rho_{deg})} \rho_{deg}^3 \left| 1 - \frac{\rho_0}{\rho_{deg}} \right|^3, \end{aligned} \quad (74)$$

where \pm stands for the light rays that turn back at $\rho_0 > \rho_{deg}$ and $\rho_0 < \rho_{deg}$ respectively.

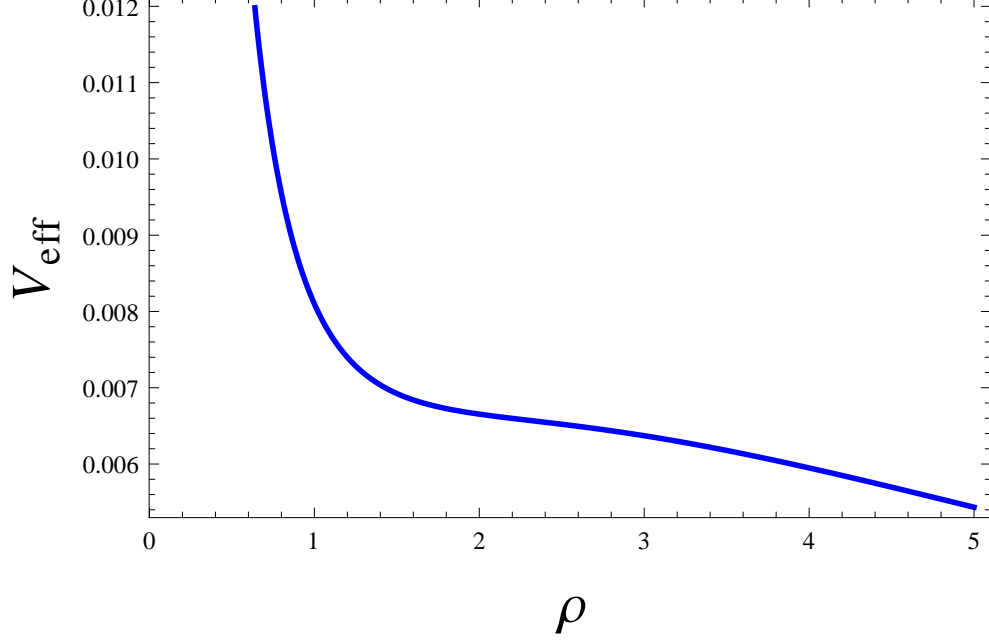


FIG. 6. Effective potential V_{eff} is plotted against ρ for the value of the parameter M below the criticality, i.e., $M < M_*$. The effective potential is monotonic function and does not admit any extremum. Thus photon sphere is absent.

Using Eqs.(18),(71),(74) we can relate θ to the deflection angle $\hat{\alpha}_0$ as

$$\theta = \frac{C_3}{D_d} + \frac{D_{3,\pm} A_{3,\pm}^3}{(\hat{\alpha}_0 + \pi - B_3)^3}. \quad (75)$$

Using Eqs.(16),(17),(75) we can compute locations of images $\theta_{3,n}$ for a given source location β in the near-aligned configuration, which are given by

$$\theta_{3,n} = \frac{C_3}{D_d} + \frac{D_{3,\pm} A_{3,\pm}^3}{((2n+1)\pi - B_3)^3} \left(1 + \frac{3}{((2n+1)\pi - B_3)} \frac{D_s}{D_{ds}} \beta \right). \quad (76)$$

For the light rays that turn back outside the photon sphere, i.e., $\rho_0 > \rho_{deg}$, since $D_{3,+} > 0$, the images are located above the critical angle $\bar{\theta}_3$ which is given by

$$\bar{\theta}_3 = \frac{C_3}{D_d}. \quad (77)$$

As n increases, images get closer and closer to $\bar{\theta}_3$ from the right side. On the other hand for the light rays that get reflected back below the photon sphere, i.e., $\rho_0 < \rho_{deg}$, we have $D_{3,-} < 0$ and the images are located below $\bar{\theta}_3$. The images get closer and tend towards $\bar{\theta}_3$ from left. The pattern of images formed is quite similar to the one depicted in the lower

panel of Fig.4. The $\theta_{3,n}$ are locations of the images formed due to the light rays that move around the lens in the clockwise sense. The location of the images $\theta'_{3,n}$ formed due to the light rays that move in the counter-clockwise sense are given by

$$\theta'_{3,n} = -\frac{C_3}{D_d} + \frac{D_{3,\pm} A_{3,\pm}^3}{((2n+1)\pi - B_3)^3} \left(-1 + \frac{3}{((2n+1)\pi - B_3)} \frac{D_s}{D_{ds}} \beta \right). \quad (78)$$

The analysis presented in this section is analytical except for the calculation of $I_{3R}(\rho_{deg})$ which is carried out numerically. In next section we discuss the case where $M < M_*$ when the black holes are far apart and no photon spheres are present.

VI. NO PHOTON SPHERE

We now deal with the final case where the parameter M is less than the critical value $M_* = \sqrt{27/8}$. Here the effective potential increases monotonically as we decrease ρ as shown in the Fig.(6). It does not admit extremum and thus there are no photon spheres. Ingoing light rays can turn back from every possible value of ρ depending on the value of the impact parameter. The divergence of the deflection angle we encountered in the sections IV and V, was intimately related to the presence of the photon sphere. But now in this case in the absence of the photon sphere the deflection angle is finite for all values of ρ_0 . It is zero for $\rho_0 = 0$ and $\rho_0 \rightarrow \infty$ and it admits maximum at some intermediate location of the turning point.

We now deal with a specific value of the parameter $M = 1.65$ and carry out a numerical computation. We numerically solve the lens equation and obtain the location of images in near-aligned configuration for source location $\beta = 0.075$ radian. Rest of the parameters are chosen in a way explained in section III. Images that appear on the right side of the optic axis are located at $\theta = 19.24, \theta = 23.81, \theta = 24.1$ and $\theta = 24.86$, whereas the images that appear on the left side of the optic axis are located at $\theta = -19.48, \theta = -23.88, \theta = -24.06$ and $\theta = -24.82$. All image locations are expressed in microarcsecond. Thus we witness a formation of finitely many, discrete, well-separated images in the absence of the photon sphere.

In the Fig.7 we have plotted $\alpha = \frac{1}{2}(\tan \theta + \tan(\hat{\alpha}_0 - \theta))$ and $\epsilon = \tan \theta - \tan \beta$ against θ . The lens equation is satisfied at the intersection of two curves and the image location for a given source location can be read off from the coordinates of the intersection point.

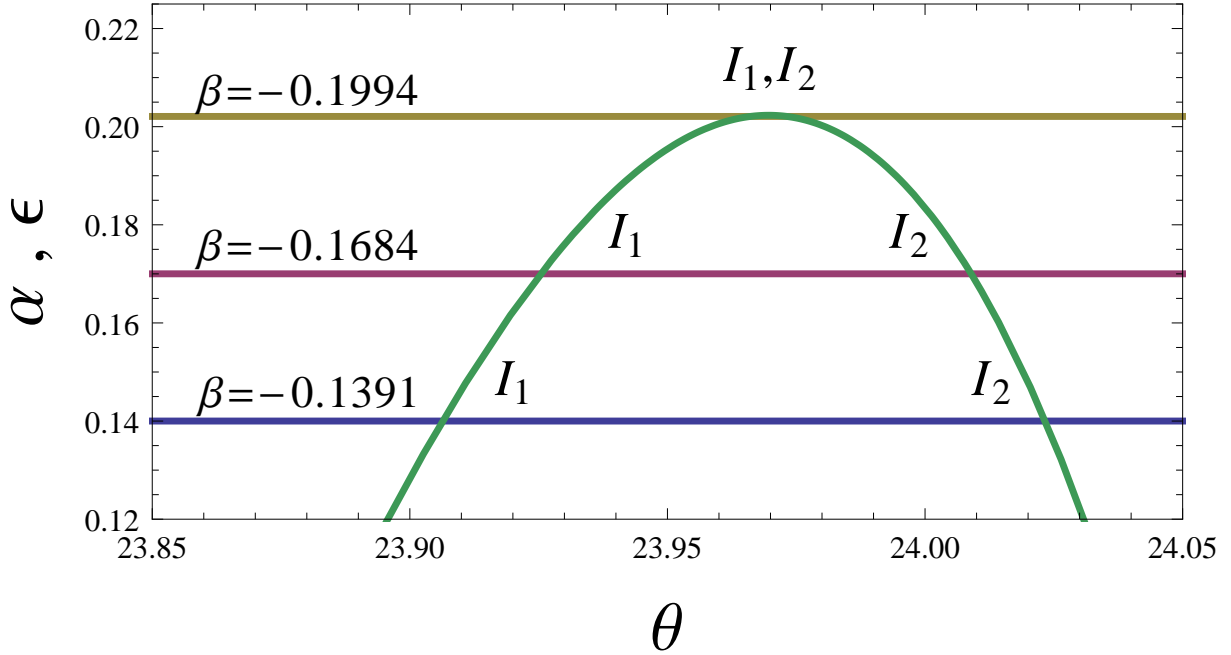


FIG. 7. $\alpha = \frac{1}{2}(\tan \theta + \tan(\hat{\alpha}_0 - \theta))$ (green curve) and $\epsilon = \tan \theta - \tan \beta$ (blue, purple and grey curves) are plotted against θ expressed in micro-arcsecond for $M=1.65$. Lens equation is satisfied when α and ϵ intersect and the image location θ can be read off from the coordinates of the intersection point. For the source location $\beta = -0.1391$ the two images denoted by I_1 and I_2 are located at $\theta_1 = 23.91$ and $\theta_2 = 24.02$. As we decrease β images move closer and for $\beta = -0.1684$, images are located at $\theta_1 = 23.93$ and $\theta_2 = 24.01$. Images move towards each other further as we decrease β and for $\beta = -0.1994$ both images coincide and a single degenerate images is located at $\theta = 23.97$. This stands for the radial caustic.

For a fixed value of β there are two intersection points as it can be seen in the figure which corresponds to the two images. Images move closer as we decrease the value of β . Two images are located at $\theta_1 = 23.91$ and $\theta_2 = 24.02$ for $\beta = -0.1391$ and for smaller value of $\beta = -0.1684$ images are located closer to one another at $\theta_1 = 23.93$ and $\theta_2 = 24.01$. Eventually two images coincide at $\theta = 23.97$ for $\beta = -0.1994$ as shown in the figure. The merger of two images separated from another in the radial direction with respect to the lens is referred to as radial caustic. Thus the radial caustic is admitted in the case where no photon sphere is present. As we can see from Fig.8, the map from image plane to source plane is degenerate at the location of radial caustic as $d\beta/d\theta = 0$.

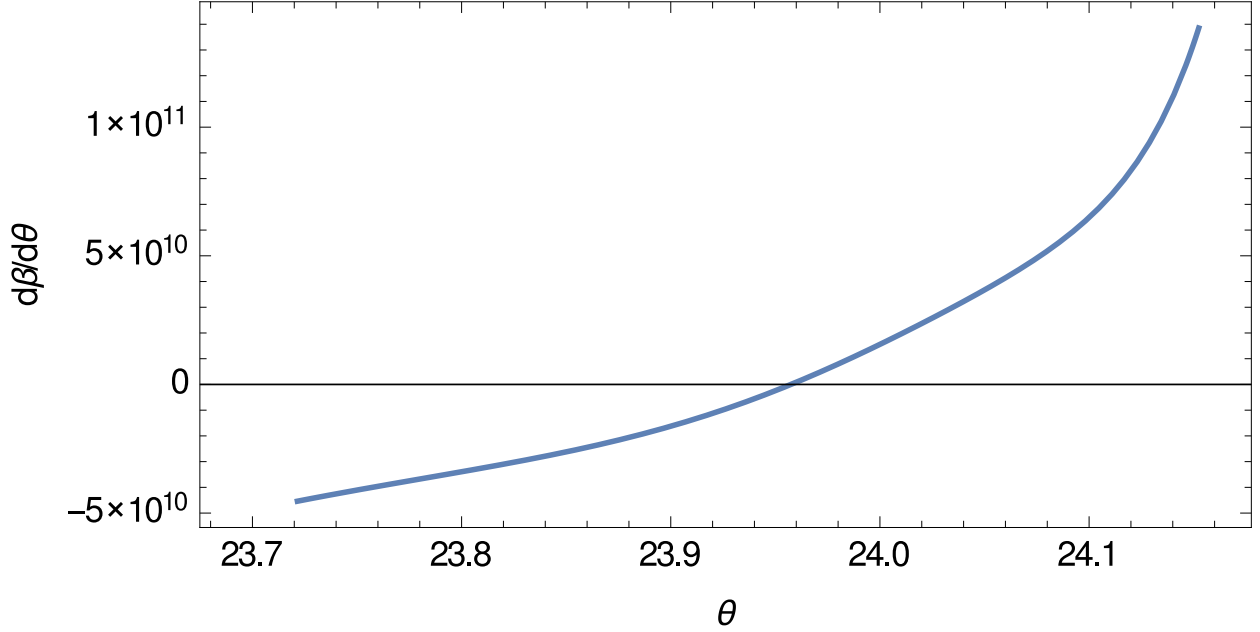


FIG. 8. $d\beta/d\theta$ is plotted against θ expressed in microarcsecond for the parameter value $M = 1.65$. The curve intersects x-axis at $\theta = 23.97$ where the map from image plane to source plane is degenerate. This is the radial caustic.

The radial caustic has never been observed before in any other investigation of relativistic gravitational lensing so far. Thus we discover a novel future in case of the binary black hole when separation between the black holes is moderately large. For a distance between black hole that is too large i.e. when $M < 1.1$ the deflection angle is small compared to 2π and thus no relativistic images are formed.

VII. CONCLUSIONS AND DISCUSSION

In this paper we studied the gravitational lensing by binary black holes. In the absence of any simple exact solution depicting the realistic binary black hole scenario, we resort to the use of Majumdar-Papapetrou metric which is the simplest multi-black hole solution in general relativity. We consider a scenario where the Majumdar-Papapetrou solution represents two equal mass maximally charged non-rotating black holes in equilibrium separated from one another by some distance. We focused on the case where the source of light and observers were located on the symmetry plane midway between the black holes and the light was

allowed to move on the plane. The central point on the symmetry plane which is also the point midway between the black hole acts a gravitational lens. The source, observer and the lens are assumed to be in the near-aligned configuration. This allows us to employ the standard techniques developed to study the gravitational lensing in the spherically symmetric spacetimes on the equatorial plane.

The photon sphere which is the circular photon orbit plays a crucial role in the relativistic gravitational lensing. The dihole spacetime can admit multiple photon spheres depending on the parameter M in the Majumdar-Papapetrou di-hole metric which is the ratio of the mass and distance between the black holes. When M is greater than the critical value given by $M_* = \sqrt{27/8}$, i.e. when for a fixed mass two black holes are located close enough, two photon spheres are present in the plane midway between the black holes. For the critical value $M = M_* = \sqrt{27/8}$, two photon spheres coincide and we have a single degenerate photon sphere located at $\rho = \sqrt{5}$. As we further increase the the parameter M beyond the critical value, i.e. when the distance between the black holes for a given mass is large enough, no photon spheres are present on the symmetry plane. The gravitational lensing signature is qualitatively different depending on whether the photon spheres are present or not.

Only one photon sphere is present in case of the single black hole. The light rays can have turning points outside the photon sphere, whereas the light rays that enter the photon sphere do not admit turning point and enter the black hole. Thus the images are formed only due to the light rays that turn back outside the photon sphere, all of which lie beyond certain critical angular radius with respect to the optic axis. There is a dark region below the critical radius. The situation is different in case of dihole due to the presence of the second photon sphere. The effective potential now turns upwards again below the second inner photon sphere and thus the light rays which enter the outer photon sphere can turn back again. A new set of infinitely many images are formed due to the light rays which enter photon sphere and turn back which are formed below the critical radius and fill up the dark void region which is present in case of the single black hole. Thus the pattern of images is drastically different in the presence of second inner photon sphere. The pattern of images in the presence of a single degenerate photon sphere is quite similar to the two photon sphere case, but the deflection angle shows power law divergence as opposed to logarithmic divergence in case of two photon spheres.

In the absence of the photon sphere the deflection angle remains finite and we witness a formation of finitely many discrete well-separated image. Interestingly we also find the presence of radial caustic i.e. as we change the source location, the two images which are separated from one another in the radial direction with respect to the lens, approach one another and eventually merge together to form a single image. The map from image plane to source plane is degenerate at that instant. The radial caustic has never been reported before in any of the investigations so far related to the relativistic gravitational lensing. Therefore we discover a novel feature in the study of binary black holes when the distance between the two black holes is above a threshold value.

The system consisting of two black holes nearby and a source of light in the vicinity could be found in the astrophysical context. The analysis carried out in this paper can potentially capture the essential features related to the gravitational lensing signature of the realistic binary black hole system. Further the new relativistic images and radial caustic can potentially introduce additional features in the microlensing light curve of binary black holes. As gravitational lensing signature is quite peculiar, it will allow us to identify the binary black hole system using electromagnetic observations. It would be possible to infer the location of the binary black hole system on the sky and also possibly distance to the source. Thus it will reduce the number of parameters in the search for gravitational waves from binary black holes in the interferometric detectors using the technique of matched filtering. This suggests that our investigation could possibly have serious implications for gravitational wave data analysis.

ACKNOWLEDGEMENTS

M.P. would like to thank S. Sahu for discussions related to two photon spheres.

-
- [1] B.P. Abbott et al., Phys. Rev. Lett. **116**, 061102 (2016).
 - [2] B.P. Abbott et al., Phys. Rev. Lett. **116**, 241103 (2016).
 - [3] J. McClintock, R. Remillard, Chapter 4 in "Compact Stellar X-ray Sources" eds. W.H.G. Lewin and M. van der Klis, Cambridge University Press.
 - [4] M. Valtonen et al., Nature **452**, 851 (2008).

- [5] S. D. Majumdar, Phys. Rev. **72**, 930 (1947).
- [6] A. Papapetrou, Proc. Roy. Irish Acad. **A51**, 191 (1947).
- [7] B. Hartle, S. Hawking, Commun. Math. Phys. **26**, 87 (1972).
- [8] A. Yumoto, D. Nitta, T. Chiba, N. Sugiyama, Phys. Rev. D **86**, 103001 (2012).
- [9] A. Wunsch, T. Muller, D. Weiskopf, G. Wunner, Phys. Rev. D **87**, 024007 (2013).
- [10] M. Patil, P. Joshi, Gen. Rel. Grav. **46**, 1801 (2014).
- [11] J. Shipley, S. Dolan, Class. Quant. Grav. **33**, 175001 (2016).
- [12] K. Virbhadra, D. Narasimha, S. Chitre, Astron. Astrophys. **337** 1-8, (1998).
- [13] K. Virbhadra, G. Ellis, Phys. Rev. D **62**, 084003 (2000).
- [14] V. Bozza, S. Capozziello, G. Iovane, G. Scarpetta, Gen. Rel. Grav. **33** 1535 (2001).
- [15] V. Bozza, Phys. Rev. D **66** 103001 (2002).
- [16] S. Sahu, M. Patil, D. Narasimha, P. Joshi, Phys. Rev. D **86**, 063010 (2012).
- [17] S. Sahu, M. Patil, D. Narasimha, P. Joshi, Phys. Rev. D **88**, 103002 (2013).